

A SPECTROSCOPIC CATALOG OF 10 DISTANT RICH CLUSTERS OF GALAXIES

ALAN DRESSLER,¹ IAN SMAIL,^{2,8} BIANCA M. POGGIANTI,^{3,6,7} HARVEY BUTCHER,⁴
WARRICK J. COUCH,⁵ RICHARD S. ELLIS³ & AUGUSTUS OEMLER JR.¹

1) The Observatories of the Carnegie Institution of Washington, 813 Santa Barbara St., Pasadena, CA 91101-1292

2) Department of Physics, University of Durham, South Rd, Durham DH1 3LE, UK

3) Institute of Astronomy, Madingley Rd, Cambridge CB3 0HA, UK

4) NFRA, PO Box 2, NL-7990, AA Dwingeloo, The Netherlands

5) School of Physics, University of New South Wales, Sydney 2052, Australia

6) Royal Greenwich Observatory, Madingley Rd, Cambridge CB3 0EZ, UK

7) Osservatorio Astronomico di Padova, vicolo dell'Osservatorio 5, 35122 Padova, Italy

Submitted: 1998 June 12; accepted: 1998 December 15

ABSTRACT

We present spectroscopic observations of galaxies in the fields of 10 distant clusters for which we have previously presented deep imaging with *WFPC2* on board the *Hubble Space Telescope*. The clusters span the redshift range $z = 0.37$ – 0.56 and are the subject of a detailed ground- and space-based study to investigate the evolution of galaxies as a function of environment and epoch. The data presented here include positions, photometry, redshifts, spectral line strengths and classifications for 657 galaxies in the fields of the 10 clusters. The catalog comprises 424 cluster members across the 10 clusters and 233 field galaxies, with detailed morphological information from our *WFPC2* images for 204 of the cluster galaxies and 71 in the field. We illustrate some basic properties of the catalog, including correlations between the morphological and spectral properties of our large sample of cluster galaxies. A direct comparison of the spectral properties of the high redshift cluster and field populations suggest that the phenomenon of strong Balmer lines in otherwise passive galaxies (commonly called E+A, but renamed here as the k+a class) shows an order-of-magnitude increase in the rich cluster environment, compared to a more modest increase in the field population. This suggests that the process or processes involved in producing k+a galaxies are either substantially more effective in the cluster environment or that this environment prolongs the visibility of this phase. A more detailed analysis and modeling of these data will be presented in Poggianti et al. (1998).

Subject headings: galaxies: clusters: general – galaxies: evolution

1. INTRODUCTION

The change with redshift observed in the proportion of star-forming galaxies in the cores of rich clusters was uncovered over twenty years ago, by Butcher & Oemler (BO, 1978, 1984), but it remains one of the clearest and most striking examples of galaxy evolution. Considerable effort has gone into acquiring photometric information that would elucidate the physical processes active in distant clusters and their effects on the evolution of both the star-forming (Lavery & Henry 1994; Lubin 1996; Rakos & Schombert 1995; Rakos, Odell & Schombert 1997) and passive galaxies (Aragón-Salamanca et al. 1993; Stanford, Eisenhardt & Dickinson 1995, 1998; Smail et al. 1998). Further impetus has been provided by observations of the recent transformation of the S0 population of clusters (Dressler et al. 1997), which may allow a closer connection to be drawn between the galaxy populations of distant clusters and the evolutionary signatures found in their local Universe counterparts (Caldwell & Rose 1997; Bothun & Gregg 1990).

However, it was the advent of spectroscopic surveys of the distant cluster populations (e.g. Dressler & Gunn 1983, 1992, DG92; Couch & Sharples 1987, CS87; Barger et al. 1996; Abraham et al. 1996; Fisher et al. 1998) which uncovered the real breadth of the changes in galaxies in these

environments, including several spectral signatures of evolutionary change, such as evidence for a strong decline in the star-formation rates of many cluster galaxies in the recent past. The advent of high spatial resolution imaging with the *Hubble Space Telescope* (*HST*) provided a further breakthrough, giving morphological information on the galaxies in these distant clusters. This could be used to link the evolution of stellar populations in the galaxies with the evolution of their *structure*, in order to understand how the various galaxy types we see in the local universe came to be. Pre- and Post-refurbishment *HST* observations by two groups (Couch et al. 1994, 1998; Dressler et al. 1994; Oemler et al. 1997) were used in early attempts to correlate spectral evolution with morphological/structural data, and to provide some insight into the mechanisms that might be driving the strong evolution in the cluster galaxy population. These two programs were extended from Cycle-4 into the “MORPHS” project, which accumulated post-refurbishment *WFPC2* images for 11 fields in 10 clusters at $z = 0.37$ – 0.56 , viewed at a time some 2 – $4 h^{-1}$ billion years before the present day.⁹ The photometric and morphological galaxy catalogs from these images were presented in Smail et al. (1997b, S97), while the data have also been used to study the evolution of the early-type galaxies within the clusters, using both color (Ellis et al. 1997) and structural information (Barger et al. 1998), the

⁸Visiting Research Associate at the Carnegie Observatories.

⁹We use $q_0 = 0.5$ and $h = 1$, where $h = H_0/100 \text{ km s}^{-1} \text{ Mpc}^{-1}$. For this geometry 1 arcsec is equivalent to $3.09 h^{-1} \text{ kpc}$ for our lowest redshift cluster and $3.76 h^{-1} \text{ kpc}$ for the most distant.

TABLE 1
TELESCOPE AND INSTRUMENT LOG

Telescope	Instrument	λ (\AA)	Spectral Scale ($\text{\AA}/\text{px}$)	Spatial Scale (arcsec/px)	# Nights	Reference
Palomar 5.1-m	COSMIC	3500–9800	3.1	0.40	19	Kells et al. (1998)
WHT 4.2-m	LDSS-2	3500–8300	5.3	0.59	6	Allington-Smith et al. (1994)
NTT 3.5-m	EMMI	3600–7800	2.3	0.27	2	Zijlstra et al. (1996)

evolution of the morphology-density relation of the clusters (Dressler et al. 1997) and the masses of the clusters from weak lensing (Smail et al. 1997a).

The aim of this paper is to combine the morphological information available from our *HST* images with detailed star-formation properties of the cluster galaxies derived from targeted spectroscopic observations. To this end we have used over 27 clear, dark nights over the past 4 years on the Palomar 5.1-m (P200),¹⁰ 4.2-m William Herschel Telescope (WHT)¹¹ and the 3.5-m New Technology Telescope (NTT)¹² to assemble a large catalog of spectroscopic data on galaxies in these clusters. We combine these new observations with previously published spectroscopy from DG92 and present spectroscopic observations of a total of 424 cluster members, of which 204 have morphologies from our *HST* imaging, as well as 233 field galaxies (71 with *HST* morphologies). In addition, we have analyzed all of the spectra to provide equivalent width measurements on a uniform system for the entire sample. The spectral catalogs, including line strength and color information, as well as the reduced spectra themselves in FITS format, are available at the AAS web site. A more detailed analysis of the spectroscopic data presented here will be given in Poggianti et al. (1998, P98).

A plan of the paper follows. We start by discussing the observations and their reduction in §2. In §3 we then give the details of the redshift measurements, as well as our analysis to quantify the strengths of spectral features and information about our spectral classification scheme based upon these. We then present the spectral properties of galaxies in the catalog and relate these to the morphologies of the galaxies from our *HST* images in §4, before discussing our results in §5. Finally in §6 we list the main conclusions of this work.

2. OBSERVATIONS AND REDUCTION

2.1. Selection of Spectroscopic Targets

The new spectroscopic observations discussed here were targeted at determining the membership of the numerous distorted and irregular galaxies revealed by our *HST* *WFPC2* images of the clusters, as well as gaining a more complete understanding of the star-formation properties of the general cluster population. With these aims, the object selection is closer to that employed by DG92, than the magnitude-limited selection criteria of CS87 and Barger et al. (1996). The latter approach has some claim to making the subsequent analysis simpler, especially when the sample is selected in the near-IR. However, it is a very inefficient method for studying the faint, blue clus-

ter members as it produces samples dominated by passive spheroidal cluster members. We chose instead to base our object selection upon galaxy morphology within the region covered by our *WFPC2* imaging, while being approximately magnitude-limited outside that area (selected from ground-based *r* or *i* CCD material to limits of $r \sim 22$ and $i \sim 21$). We note at this point that two of the cluster fields, A 370 Field 2 and Cl0939+47 Field 2, lie outside of the central regions of their respective clusters (although we do also have observations of the core regions as well). The difference in the galaxy density between the fields should be kept in mind in the following analysis, although we will highlight such selection effects for individual figures when they are discussed below. Modelling of the sample selection for the entire spectroscopic catalog is dealt with in more detail in P98.

2.2. Spectroscopic Observations

The spectroscopic observations discussed in this paper were undertaken with a variety of facilities over the period 1993–1997. We list the instruments and telescopes employed and the total number of nights used in Table 1. The basic details of the 10 clusters targeted in this study are listed in Table 2, this includes the mean cluster redshift, the one dimensional velocity dispersion (σ_{cl} , see §3.2), the redshift range used to define cluster membership (Δz), the field center and the *HST* *WFPC2* filters used in the observations. The new spectra presented here are typically of high quality due to both the long exposure times employed in our observations and the combination of the high efficiency of the multi-object spectrographs and the large aperture of the telescopes used. We give in Table 3 the logs of the observing runs for the various telescopes. We list the mask identification, the dates of the observations, the total exposure time and the number of objects extracted from each mask (N). The slit width typically used was 1.5 arcsec, with slits between 10–20 arcsec long. The exact size of the region on the slit used to extract the galaxy spectrum depended upon the relative signal to noise of the galaxy spectrum, but varied between 1.1–8.4 arcsec for the COSMIC spectra with a mean length of 3.9 ± 1.2 arcsec. At the median redshift of the clusters in our catalog, the spectra thus sample a physical scale of $\sim (5 \times 13)h^{-1}$ kpc.

The exact details of the extraction and reduction of the spectra depends upon the instrument and set-up used. However, the basic steps were the same for all the data and we outline the procedures used for both the COSMIC and WHT/NTT data. The raw frames were debiased using the over-scan regions on the chip, before being trimmed. A

¹⁰The Hale 5-m of the Palomar Observatory is owned and operated by the California Institute of Technology.

¹¹The William Herschel Telescope of the Observatorio del Roque de los Muchachos, La Palma, is operated by the Royal Greenwich Observatory on behalf of the UK Particle Physics and Astronomy Council.

¹²Based in part on observations collected at the European Southern Observatory, La Silla, Chile.

TABLE 2
PROPERTIES OF THE CLUSTERS

Cluster	z	σ_{cl} (km s^{-1})	Δz	R.A. (J2000)	Dec. (J2000)	<i>HST</i> Filters	Comment
A 370	0.3741	1170	0.3589–0.3873	02 39 52.6	−01 34 18	F555W/F814W, F702W	Center (F702W), outer field (F555W/F814W)
Cl 1447+26	0.3762	1470	0.3621–0.3857	14 49 29.3	+26 07 52	F702W	
Cl 0024+16	0.3928	1150	0.3755–0.4081	00 26 35.7	+17 09 46	F450W/F814W	
Cl 0939+47	0.4060	1260	0.3879–0.4173	09 42 56.1	+46 59 12	F555W/F814W, F702W	Center (F702W), outer field (F555W/F814W)
Cl 0303+17	0.4184	1310	0.4018–0.4338	03 06 12.9	+17 20 08	F702W	
3C 295	0.4593	1630	0.4464–0.4733	14 11 10.5	+52 12 11	F702W	
Cl 0412−65	0.5074	700	0.5024–0.5130	04 12 50.1	−65 50 44	F555W/F814W	
Cl 1601+42	0.5388	1210	0.5100–0.5473	16 03 12.0	+42 45 26	F702W	
Cl 0016+16	0.5459	1660	0.5300–0.5601	00 18 33.3	+16 26 16	F555W/F814W	Spectra from DG92
Cl 0054−27	0.5608	1180	0.5520–0.5770	00 56 59.0	−27 40 20	F555W/F814W	

two dimensional flatfield was constructed by dividing the flatfield exposure by a low-order fit in the dispersion direction. The data frame was then divided by this normalized flatfield, this served to correct for the pixel-to-pixel response of the detector. The sequence of data frames for each mask taken on a single night were then checked for spatial offsets between the exposures arising from flexure in the spectrograph (these are typically only $\lesssim 0.2$ pixels for COSMIC in the course of a night). If necessary the exposures were shifted in the spatial and/or dispersion direction to align them and then combined with a cosmic-ray rejection algorithm using the IRAF task IMCOMBINE. This produced a two dimensional image of the mask exposure clean of cosmic ray events. These frames were then geometrically remapped to align the spectra along the rows of the detector. This step is necessary to remove the distortion of the spectra on the detector introduced by the spectrograph optics. The distortion is only a large effect for objects in slits near the edge of COSMIC’s large $13.7' \times 13.7'$ field of view, although aligning the spectra also helps when tracing some of the faintest objects. The distortion of the spectra are mapped using the positions of the emission lines in the arc exposure taken after every science exposure. The positions of objects in each slit on the remapped frame, as well as regions of clear sky surrounding them, were then defined interactively using the IRAF package APEXTRACT. The exact position of the object within the slit was traced in the dispersion direction and fitted with a low-order polynomial to allow for atmospheric refraction. The spectra were then sky-subtracted and extracted using optimal weighting to produce one dimensional spectra. The arc exposures associated with each science exposure were remapped and extracted in exactly the same manner (although with no sky-subtraction) and these were used to determine the wavelength calibration for the science exposure. We estimate our wavelength scale is good to 0.2\AA rms. Finally, the one dimensional spectra were smoothed to the instrumental resolution, $\sim 8\text{\AA}$, and rebinned to 10\AA per pixel to make them more manageable. The spectra obtained with COSMIC have not been flux calibrated.

The WHT and NTT spectra have been reduced using the LEXT package, purposely written for reducing LDSS–2 spectra, and the MIDAS software package. What follows is a brief description of the reduction procedure generally adopted. A number of twilight and dome flatfields, and several arc frames were obtained for each mask, as well as numerous bias frames and long–slit spectra of standard

stars for flux calibration (at least one star per night). The raw frames were first debiased and then divided by the corresponding normalized flatfield. They were then calibrated in wavelength with the arcs frames obtained either with a CuAr or HeArNe combination of lamps. The sky–subtraction step was performed with an interactive choice of the spatial limits of the spectrum, which was then extracted summing the counts weighted with a Gaussian. The long–slit stellar spectrum was reduced in a similar way as the target spectra and a response function was derived by the comparison with a tabulated spectrum. Each spectrum was flux–calibrated in F_ν by dividing for this response function. In the case of the WHT and NTT spectra each exposure of a given mask was reduced and calibrated separately, before all the spectra of a given galaxy were coadded; no smoothing or rebinning was applied.

The full digital catalog of FITS spectra collected for this program is distributed in electronic form on the AAS web site. These spectra are also available from: <http://www.ociw.edu/~irs>.

3. SPECTROSCOPIC ANALYSIS

The full catalog of objects observed spectroscopically in the 10 clusters is given in Tables 4 (the complete tables are included on the AAS web site as well as being available from <http://www.ociw.edu/~irs>). This has been split into “Cluster” and “Field” samples as described below. The tables list not only the spectral information on the galaxies, but also any available morphological and photometric data from S97 and DG92. A key to the various parameters and the format of the tables are given in Table 5. We now describe in more detail the measurement of some of the spectral parameters listed in Tables 4.

3.1. Spectral Measurements

The quality of the spectra, both in terms of signal-to-noise and sky-subtraction, was visually assessed by AD for *all* of the spectra presented. The spectra are graded on a 4–point range, with $q = 1$ signifying the best and $q = 4$ the worst quality. Of the complete catalog 17% have $q = 1$, 47% with $q \leq 2$ and 89% are $q \leq 3$. Spectra with $q \leq 3$ have sufficient signal to noise (S/N) for not only measurement of a redshift, but also to quantify the strength of any spectral features present. From the continuum regions around the [OII] $\lambda 3727$ and H δ lines we estimate median S/N of 40.2 ($q = 1$), 28.3 ($q = 2$) and 19.7 ($q = 3$), with lower limits to the S/N of 20.9, 10.6 and 4.6

TABLE 3
LOG OF NEW SPECTROSCOPIC OBSERVATIONS

Target/Mask	Date	Exposure time (ks)	N	Comments
COSMIC/P200				
Cl 0024+16 EW-1	5-6 Aug 1994	18.8	37	
Cl 0024+16 EW-2	29 Nov 1994, 1-3 Dec 1994	20.8	34	
Cl 0024+16 NS-1	29-30 Oct 1994	27.0	35	
Cl 0024+16 NS-2	19 Aug 1995, 25-26 Sept 1995	20.0	29	
A370 MS-1	25-26 Sept 1995	10.8	25	
A370 MS-2	27-28 Nov 1995	24.0	29	
A370 MS-3	4 Oct 1997	16.2	22	
Cl 0303+17 EW-1	29 Nov 1994, 1 Dec 1994	25.0	30	
Cl 0303+17 EW-2	2 Dec 1994	15.0	30	
Cl 0303+17 NS-1	3 Dec 1994	15.0	27	
Cl 0939+47 NS-B	13 Dec 1993	10.8	18	Using 'old' COSMIC CCD
Cl 0939+47 EW-B	29-30 Nov 1994, 1 Dec 1994	38.2	35	
Cl 0939+47 EW-F	1-2 Dec 1994, 24 Feb 1995	36.0	34	
Cl 1601+42 CM-1	28-29 May 1997	22.2	20	
Cl 1601+42 CM-2	18-19 June 1996	21.6	22	
Cl 1601+42 CM-3	11-12 May 1997, 29 May 1997	30.2	24	
LDSS-2/WHT				
Cl 0939+47 WA-1	24 Mar 1993	14.4	10	
Cl 0939+47 WA-2	25 Mar 1993	14.4	7	
Cl 0939+47 WA-3	26 Mar 1993	10.8	7	
Cl 0939+47 WA-4	26 Mar 1993	9.0	6	
Cl 0939+47 MA-A,MA-D	27-28 Apr 1995	9.0	10	
Cl 0939+47 MB-A,MB-D	29 Apr 1995	9.0	7	
3C 295 MA-A,MA-D	27 Apr 1995	9.0	6	
Cl 1447+26 WA-1	25-26 Mar 1993	10.8	23	
Cl 1447+26 MA-A,MA-D	28-29 Apr 1995	12.6	9	
Cl 1601+42 MA-A,MA-D	28 Apr 1995	9.0	8	
EMMI/NTT				
Cl 0054-27 MA-1	23 Nov 1995	10.2	15	
Cl 0054-27 MA-2	24 Nov 1995	10.8	21	
Cl 0412-65 MA-1	23 Nov 1995	9.0	15	
Cl 0412-65 MA-2	24 Nov 1995	8.6	21	

respectively for these three quality classes. Repeated observations suggest that the redshifts of $q = 1$ and $q = 2$ cases are correct at a confidence of greater than 98%, and that $q = 3$ cases are correct at a confidence of greater than 90%. In contrast, those spectra with $q = 4$ are of sufficient S/N to provide only a redshift, which may be uncertain in a significant number of cases.

Redshifts were measured from the spectra interactively using purpose-written software that compares the wavelengths of redshifted absorption and emission lines with features in the spectra. Whenever possible we used a number of features to estimate the redshift, and only in a very small number of cases is a redshift based on only a single feature — these instances are noted in the comments in Tables 4. We list in column 24 of Tables 4 the main features used to identify the galaxy redshifts. For conciseness we have used the following abbreviations to identify the lines: Babs, Balmer absorption lines; Ha, H α ; Hb, H β ; Hd, H δ ; He, H ϵ ; Heta, H η ; Hg, H γ ; Hth, H θ ; Hz, H ζ ; G, G-band; H&K, Ca H or K; Mg, Mg-B; Na, Na-D; OII, [OII] λ 3727; OIII, [OIII] λ 4959,5007; bk, 4000 \AA break; MgII, MgII λ 2799; CIII, CIII λ 1909; CIV, CIV λ 1549; FeI, FeI λ 5268; NII, [NII] λ 6583; SII, [SII] λ 6716,6731.

The strength of emission and absorption features in the spectra were measured using purpose-written software, allowing the positioning of the continuum to be defined interactively. We give the restframe equivalent widths (EW) for [OII] λ 3727 and H δ in columns 5 and 6 of Table 4A and 4B, in all instances a line seen in emission is given a negative value and is quoted in \AA . The presence and

strength of these lines is used in the spectral classification scheme discussed in §3.2. If other lines in the spectrum were measurable we list their EW in the comments. We give line strengths for not only those galaxies observed for this work, but also those from the early survey of DG92. The D4000 measurements have been similarly placed on a consistent system. These are measured using wavelength intervals as defined in Dressler and Shectman (1987). The COSMIC data shared a common relation of counts to flux, but were not flux calibrated per se. A multiplicative correction of 1.34 to convert the measured D4000 to true D4000 for these data was derived by comparing the COSMIC spectra of repeated objects with the equivalent flux calibrated DG92 spectra. This procedure, though imperfect, generates reasonable and consistent results, as shown by multiple COSMIC observations of the same galaxies.

We have a total of 31 repeat observations, both internally within the datasets from a single telescope, and between telescopes. We find median rms scatters of $\sigma(z_{\text{COSMIC}} - z_{\text{DG92}}) = 0.0018$ ($N = 14$), $\sigma(z_{\text{COSMIC}} - z_{\text{WHT}}) = 0.0009$ ($N = 2$) and $\sigma(z_{\text{COSMIC}} - z_{\text{COSMIC}}) = 0.0005$ ($N = 7$) for those spectra with $q \leq 3$, and no systematic offsets between any of the individual datasets: $\langle z_{\text{COSMIC}} - z_{\text{DG92}} \rangle = 0.0007$, $\langle z_{\text{COSMIC}} - z_{\text{WHT}} \rangle = -0.0009$. We therefore conclude that there are no significant offsets between the redshifts from the different datasets and hence we are confident that we can include all the observed objects in our analysis.

Finally, we quantified the detectability of [OII] and H δ in our spectra. This enabled us to derive the lower lim-

TABLE 5
NOTES ON THE PARAMETERS IN TABLES 4

Column	Parameter	Units	Format	Comment
1.....	CLUSTER		A6	Cluster
2.....	ID		I4	ID in spectroscopic catalog for cluster
3.....	z		F7.4	Redshift
4.....	Q		A1	Redshift quality – a “:” indicates questionable identification
5.....	[OII]	Å	I2	Quality of spectrum: 1=High, 4=Low.
			F7.1	Restframe equivalent width of [OII] 3727
6.....	H δ	Å	A1	Quality of [OII] 3727 EW measurement (a “:” indicates questionable)
			F4.1	Restframe equivalent width of H δ , –ve indicates emission
7.....	D4000		A1	Quality of H δ EW measurement (a “:” indicates questionable)
8.....	CLASS		F5.2	Break strength index
9.....	δ RA	arcsec	A11	Spectral classification in scheme described in §3.3
10.....	δ Dec	arcsec	F7.1	RA offset from field center in Table 2
11.....	ID _{HST}		F7.1	Dec offset from field center in Table 2
12.....	X	Pixels	I5	ID in photometric catalog for cluster ^a
13.....	Y	Pixels	I5	X coordinate on <i>WFPC2</i> frame ^a
14.....	MORPH		I5	Y coordinate on <i>WFPC2</i> frame ^a
15.....	T		A12	Galaxy morphology ^a
16.....	D		I2	T-type ^a
17.....	INT		I2	Visual disturbance index ^a
18.....	MAG	Mag	A6	Interpretation of disturbance ^a
19.....	COL	Mag	F5.2	Total magnitude in F702W/F814W from <i>WFPC2</i> frame ^{a,b}
20.....	MAG _{DG}	Mag	F5.2	Aperture color from <i>WFPC2</i> frame ^{a,c}
21.....	COL _{DG}	Mag	F6.2	Magnitude from ground-based imaging published in DG92 ^d
22.....	RUN		F6.2	Color from ground-based imaging published in DG92 ^d
23.....	MASK		A6	Code giving details of observing run ^e
24.....	FEATURES		A10	Mask and object slit identifier
25.....	COMMENTS		A23	Spectral features identified, see §3.1
			A130	Description of features in spectrum

^a See S97 for more details.

^b Magnitudes are in F702W for Cl0303+17, Cl0939+47, 3C295, Cl1447+26 and Cl1601+42, and in F814W for Cl0016+16, Cl0024+16, Cl0054–27, A370 Field 2, Cl0412–65, Cl0939+47 Field 2.

^c *WFPC2* $V_{555} - I_{814}$ color information is available for: Cl0016+16, Cl0054–27, A370 Field 2, Cl0412–65, Cl0939+47, and $B_{450} - I_{814}$ colors for Cl0024+16.

^d Aperture r -band magnitude from DG92, colors are aperture ($g - r$) measurements in all instances.

^e [P/W/N]<MONTH><YEAR>, P=Palomar 5-m, W=WHT, N=NTT, or DG92.

its on the strength of these spectral features below which we would not have identified them. Achieving this aim was not straightforward because the code that best measured the equivalent widths, which is based on a gaussian line-fitting program written by Paul Schechter, does not perform well when the lines are weak or undetectable. For this reason, when we measured the strengths of features in those galaxies where the feature was not clearly seen, we by necessity had to measure equivalent widths using the standard technique of obtaining the continuum level from straddling continuum bands, and measuring the decrement or increment in signal relative to the continuum in an interval containing the feature. We made such measurements of [OII] and H δ EW for all COSMIC spectra with qualities $q \leq 3$ of cluster members in Cl0939+47 and Cl0024+16, a total of 79 galaxies. The intervals are, again, as defined in Dressler and Shectman (1987). For weak, but measurable, cases the line-fitting and flux-summing techniques give equivalent results, though for strong absorption lines, in particular, the latter seems to underestimate the strength of the feature, apparently by allowing the wings of the line to lower the continuum level. We believe, however, that the two scales for measuring equivalent widths are interchangeable for the purpose of looking for weak features.

The results of these tests are shown in Fig. 1a and Fig. 1b, where we have plotted the equivalent widths as a function of signal-to-noise ratio in the continuum bands straddling the feature. In Fig. 1b we show that the galaxies that were designated by inspection as emission line types all have [OII] EW stronger than -3\AA , while those designated as having no emission lines (spectral types: k, k+a,

or a+k, see §3.3) have [OII] EW weaker than -4\AA . In fact, the latter are consistent with non-detections: for 37 non-emission line members, the median EW is $+0.4\text{\AA}$ with quartiles of -1.0 to $+2.6$. There is only a weak trend with signal-to-noise ratio. We conclude from these data that we are complete for [OII] stronger than -5\AA , with a high level of completeness down to -3\AA . In other words, even at the modest signal-to-noise ratios of these spectra, none of the galaxies classified as non-emission types are likely to have emission at greater than the -3\AA level, and certainly none have emission stronger than -5\AA (this limit corresponds to “absent” in Table 6).

In Fig. 1b we show a similar diagram for the same sample, this time for H δ . Because it is weaker and in absorption, H δ is a more difficult feature to measure; this is apparent from the stronger trend with signal-to-noise ratio. However, as for [OII], the separation of those galaxies which are designated by inspection as having moderate Balmer line strengths (k+a, a+k, and e(a), see §3.3) from the non-Balmer galaxies (k and e(c) and e(b) types), is confirmed by the objective measurements. The boundary is around $2-3\text{\AA}$, below which point we are unable, except at high S/N > 50 , to discern the difference between the presence or absence of H δ . We conclude from these data that we are complete above equivalent widths of $+5\text{\AA}$, and mostly complete above $+3\text{\AA}$. It is worth commenting that some of the points with large negative equivalent widths for H δ arise from strange continuum levels, rather than from the feature seen in emission (although there is at least one clear case of H δ in emission, a rare phenomena among luminous galaxies).

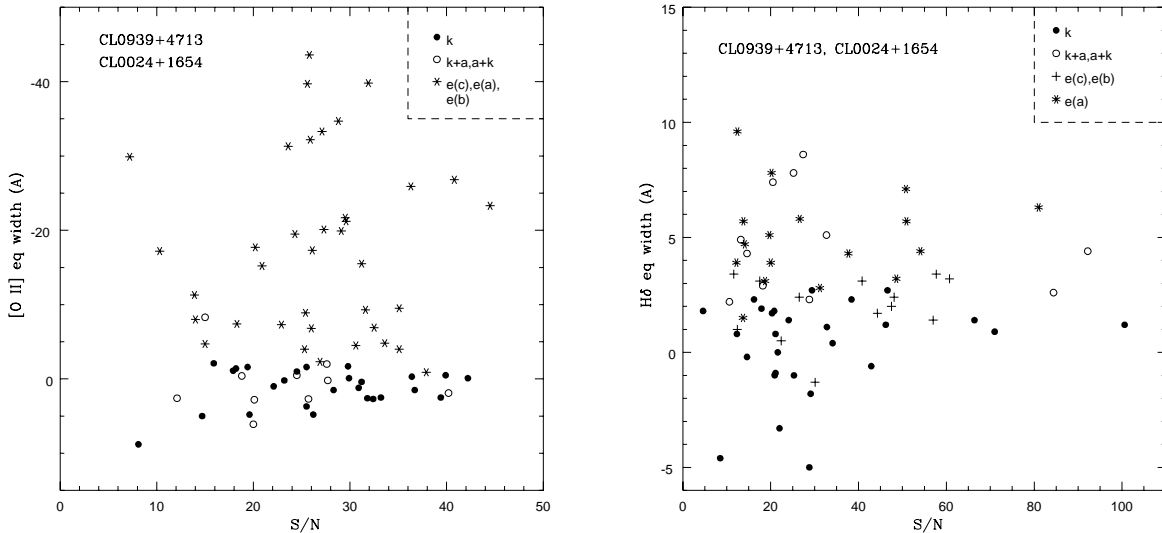


Fig. 1. a) Measured [OII] equivalent widths versus the S/N in the straddling continuum. The data are for 79 cluster members with $q \leq 3$ in the clusters CL0939+47 and CL0024+16. There is a clean separation at $\sim -4\text{\AA}$ between the types for which [OII] was found by inspection and those for which it was judged to be absent. b) The equivalent plot for the measured H δ equivalent widths. H δ strengths greater than 3\AA are clear detections, according to the distribution, with $2\text{--}3\text{\AA}$ strengths ambiguous, particularly at low S/N.

3.2. Cluster Membership

As was noted above, Table 4 is split into two parts on the basis of whether a galaxy is classed as a “Cluster” member or “Field”. To accomplish this we define redshift ranges for the various clusters; these ranges are purposefully chosen to be large to ensure that we retain any galaxies in the large-scale structure surrounding the clusters, while at the same time minimizing the contamination by field galaxies. In Fig. 2 we show the redshift distributions for the individual cluster fields; in each panel the inset provides a more detailed view of the velocity distribution close to the cluster mean. The bin size in these plots has been arbitrarily chosen and may artificially enhance or suppress the visibility of any structures within the clusters. We list the resulting mean redshift, restframe velocity dispersion and redshift range defining each cluster in Table 2. We reiterate that the velocity dispersions are likely to be overestimates of the true dispersion of the well-mixed cluster population. We also list in Table 2 the number of member galaxies in our catalog for each cluster. Using these definitions our catalog contains a total of 424 cluster members and 233 field galaxies.

The redshift distribution for all galaxies classed as field is shown as the open histogram in Fig. 3; the galaxies with *HST* morphologies are shown as the filled histogram. The median redshift of the whole field sample is $\langle z \rangle = 0.42$, while for the morphological sub-sample it is slightly higher at $\langle z \rangle = 0.46$ (Fig. 3). These values are very similar to the median redshift of our 10 clusters, $\langle z \rangle = 0.44$, allowing us to easily compare the broad properties of the cluster and field samples. A total of 20 stars were observed (all in either the flanking fields or from the earlier DG92 observations); these are included at the bottom of Table 4b, but we do not discuss them further.

In Fig. 3 we may be seeing some evidence for a deficit in the total field redshift distribution, between $z \sim 0.4\text{--}0.6$, which would result from the inclusion of a few field galax-

ies in the cluster catalog. This would include galaxies in the supercluster environment, if any, in which the clusters reside, or truly unassociated galaxies relatively far from the cluster but within the wide velocity limits imposed by the cluster’s velocity dispersion. To estimate the extent of this effect we use two approaches. Firstly, a conservative upper limit on the deficit comes from linearly extrapolating the trends of number versus redshift in the field at $z < 0.35$ and $z > 0.60$ to limit the likely number of field galaxies in the intervening redshift range. From this we estimate that there should be $\lesssim 160$ field galaxies in the range $z = 0.3\text{--}0.6$, compared to the observed number of 92, giving an upper limit on the deficit of ~ 70 galaxies, or $\lesssim 7$ per cluster. Alternatively, using the regions where the redshift limits of the cluster and field samples overlap between different clusters we estimate the contamination from random, unrelated field galaxies is of the order of 1.0 ± 0.7 galaxies per cluster in our largest velocity range. We conclude therefore that the contamination from galaxies unrelated to the cluster, or its supercluster, does not exceed 7 galaxies per cluster and is probably closer to 1–2 galaxies.

3.3. Spectral Classification

To assess the distribution in the star-formation properties of galaxies in our catalog we have found it useful to classify their spectra into a number of classes. These classes are broadly based upon those used by DG92 and CS87, however, the number of classes has been expanded to better cover the full range of features seen in our large sample. We have also used the properties of low redshift integrated spectra (Kennicutt 1992) and the expected characteristics from spectral modelling to help us define the limits of some of the classes. In revising the classifications we therefore found it necessary to redefine some of the boundaries previously used for the spectral classes. Hence, to reduce confusion between our new classes and

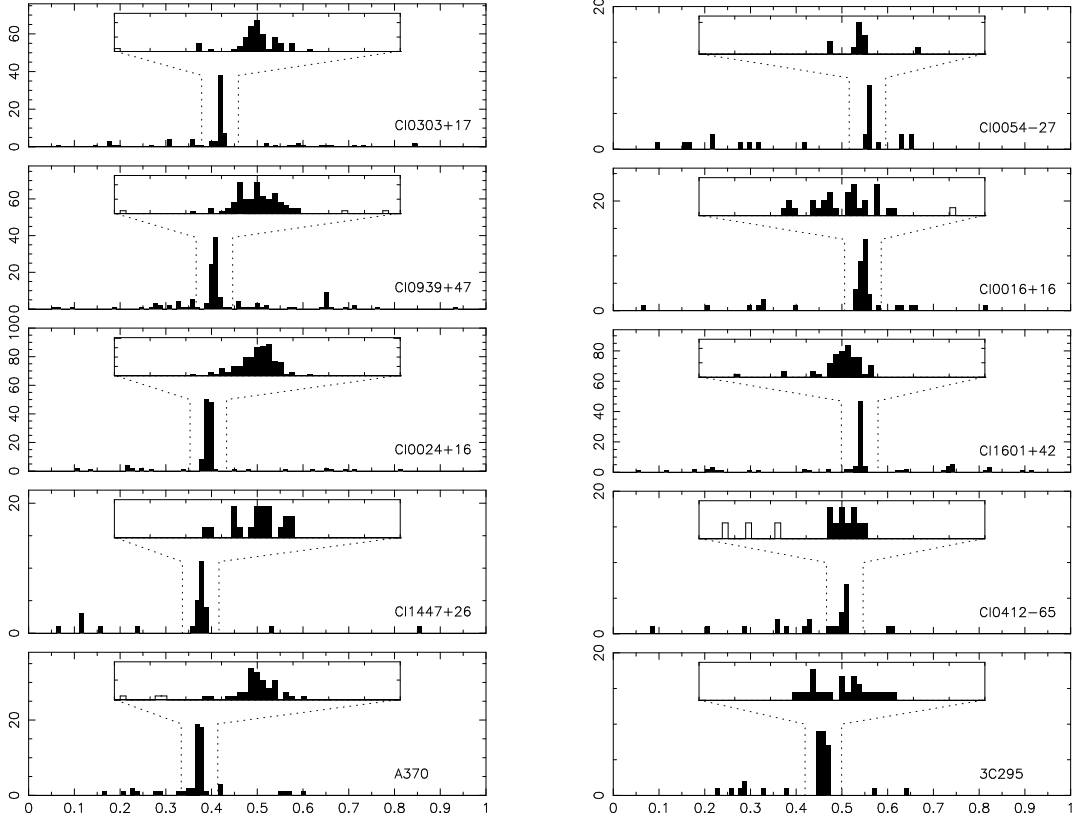


Fig. 2. Redshift distributions for the fields of our 10 clusters. We show the redshift range $z = 0-1$ in the full plot and then, in the insets, an expanded region (width $\Delta z = 0.08$) centered on the cluster redshift, in the inset panels we show the cluster members as a filled histogram and the field galaxies as open. The redshift axis in the inset panel is marked with $\Delta z = 0.01$ increments and the vertical axis is the same as the main panel.

those used previously we adopt a new nomenclature and give this and the details of the classification scheme in Table 6. We show a schematic representation of this spectral classification in Fig. 4. It should be noted that for those spectra where sky residuals or the available spectral range precluded the observation of one of the diagnostic spectral features, we have made use of the strength of the other Balmer series lines (if $H\delta$ was unobservable) or emission lines (if $[OII]$ was unobservable) to identify the most likely spectral class. In the few cases where this has been done comments are included in Table 4.

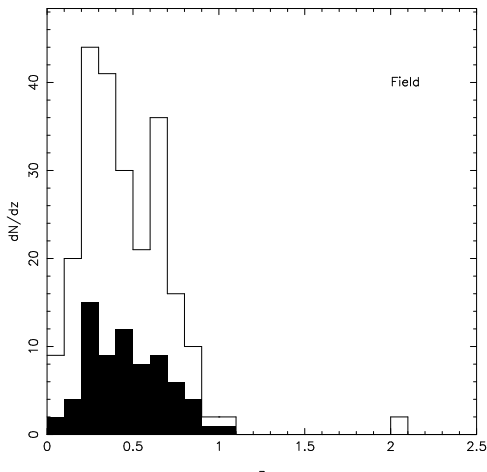


Fig. 3. Redshift distribution for galaxies classified as non-members in the fields of the 10 clusters. The open histogram gives the total redshift distribution for the field galaxies (233 galaxies), the filled histogram is those field galaxies which lie within the *WFPC2* field and for which we

therefore have detailed morphological information (71 galaxies).

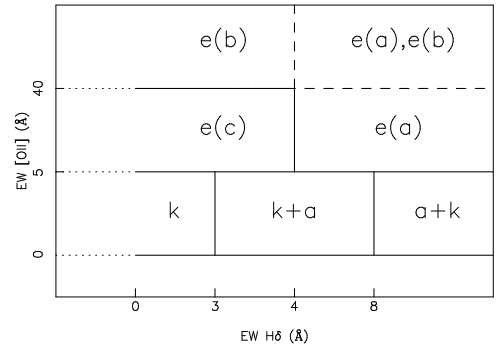


Fig. 4. A schematic representation of the spectral classification scheme used in this work. We show the regions of the $H\delta$ - $[OII]$ equivalent width plane populated by the various spectral types. Those spectral classes not based on the line strengths of $H\delta$ and $[OII]$ (e.g. CSB, e(n), etc.) are not marked.

Briefly the overlap between the new system and previous ones can be summarized as follows: we retain the general features of the DG92 system, including k-type and the general class of “e” (emission) galaxies. However, we replace the mixed nomenclature “E+A” with k+a (following the suggestion of Franx 1993) and a+k, depending on the strength of the $H\delta$ Balmer line. We also subdivide emission line galaxies into e(a) types (with strong Balmer absorption), e(c) for those with weak or moderate Balmer absorption, and e(b) for those with very strong $[OII]$ (this can sometimes be combined with e(a) for galaxies with both strong $[OII]$ emission and strong Balmer absorption). This nomenclature reflects the nature of the spectra, with

e(a) indicating a population of A stars, e(b) a spectrum similar to that expected for a burst of star-formation and e(c) a spectrum for a system undergoing a more constant SFR.

In comparison to other earlier work, the PSG and the HDS galaxies of CS87 fall mostly into the a+k and k+a classes. The CS87 ‘‘Spiral’’ types are placed in e(c) and e(a); however, the SB galaxies are not the same as our type e(b), because the criteria for these in CS87 was not based on [OII] strength. We note that spectral classes described in Table 6 can be grouped in three main categories: passive (k); past star-forming (k+a and a+k) and currently star-forming (e(c), e(a) and e(b)). AGN spectra (e(n)) are excluded in this division (Table 6).

In Column 8 of Table 4 we include a photometric classification in the case of the bluest galaxies. These are labeled ‘‘Color Starburst’’ (CSB) if their restframe color is bluer than that expected for a low metallicity model galaxy with an increasing star-formation rate (P98). This allows us to conservatively identify those galaxies whose very blue colors can only be explained with a current starburst, whatever their spectral type may be.

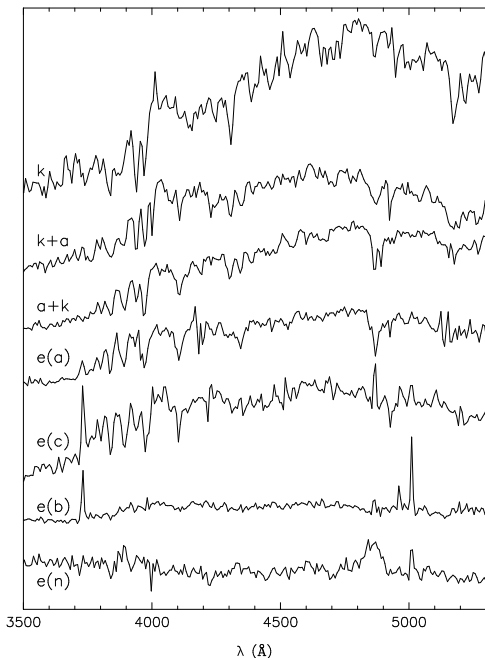


Fig. 5. Representative spectra from each of the spectral classes in our adopted scheme (Table 6, Fig. 4). These are plotted with arbitrary vertical scaling and in the restframe. The galaxies are all cluster members with $q = 1$ and come from Cl 0939+47 and Cl 0024+16. The spectra are not fluxed.

To better illustrate the properties of the new classification scheme we show in Fig. 5 a high-quality, representative member of each class from our catalog. In Table 7 we give the distribution of spectral classes within the different clusters (for $q \leq 4$), as well as the total numbers across all the clusters and the equivalent values for our field samples. As can be seen, the clusters are populated by a wide variety of spectral classes, although comparisons between clusters are not simple owing to the different apparent magnitudes of the samples and the attending variation in the typical quality of the spectra. Table 7 also lists the equivalent numbers of galaxies in each spectral class for which we have morphological information.

4. BASIC PROPERTIES AND CORRELATIONS OF THE DATA

To start the discussion of the spectroscopic sample we have assembled, we review the basic properties of the sample as a whole. We focus on a few of the correlations between the various properties of the galaxies in the sample, in particular the relationships between the morphological, spectral, and kinematic characteristics of certain classes of cluster galaxies. In the following discussion we will include the uncertain spectral classes (marked with a ‘‘:’’ in Tables 4), unless otherwise stated.

4.1. Luminosity Functions for the Morphological Classes

In order to draw conclusions from our spectroscopic study in the context of the broader morphological catalog (S97), we need to compare the sampling in absolute magnitude of the two catalogs. Fig. 6a shows the absolute magnitude distribution for galaxies in the spectroscopic catalog for which ground-based r -band photometry is available. This filter approximates V in the restframe for all 10 clusters. Our assumption of a single K -correction (from an spectral energy distribution (SED) corresponding to a present day Sbc) introduces only small errors into the magnitude distribution ($\lesssim 0.06$ mags for E/S0 and Sd/Irr SED). Fitting a Schechter function to the bright-end of the distribution in Fig. 6a, we obtain a characteristic magnitude of $M_V^* = (-20.64 \pm 0.16) + 5 \log_{10} h$ (for a fixed faint-end slope of $\alpha = -1.25$ as adopted in S97). This is to be compared to a fit obtained to the morphological counts in the cluster fields corrected for likely contamination in the manner described in S97. Fitting to the composite luminosity function of all morphological types across the 10 clusters we find $M_V^* = (-20.79 \pm 0.02) + 5 \log_{10} h$ (for $\alpha = -1.25$). This good agreement indicates that the spectroscopic catalog fairly samples the morphological catalog for $M_V < -19 + 5 \log_{10} h$.

Fig. 6b shows how the spectroscopic sampling compares as a function of morphological type within the clusters. This is achieved by comparing the spectroscopic sample for $M_V < -19 + 5 \log_{10} h$ to the field-corrected morphological counts of S97. There is no significant trend with morphological type except for the selection effect, discussed in §2.1, built into the original sample selection: the Sd/Irregular galaxies are oversampled relative to the E–Sc types (although there is considerable uncertainty in the statistical correction for field galaxies in this bin, S97). This plot allows us to quantify and correct for the sample selection in our analysis as required.

4.2. Luminosity Functions for the Spectral Classes

The absolute magnitude distribution of the spectral classes defined in this paper will be important to understanding their relationships within the framework of galaxy evolution models. Fig. 7a shows that the magnitude distributions brighter than $M_V = -19 + 5 \log_{10} h$ for spectral classes k, k+a and a+k are statistically indistinguishable. In contrast, the e(a) and e(c) classes appear to systematically fainter than the k class; this difference is confirmed at the $\gtrsim 95\%$ confidence limit using two-sample Kolmogorov-Smirnoff tests. It is important to keep in mind the ‘‘completeness’’ limit of the spectroscopic catalog

TABLE 6
SPECTRAL CLASSIFICATION SCHEME

Class	EW [OIII] 3727 (Å)	EW H δ (Å)	Color	Comments
k	absent	< 3	...	passive
k+a	absent	3–8	...	moderate Balmer absorption without emission
a+k	absent	≥ 8	...	strong Balmer absorption without emission
e(c)	yes, < 40	< 4	...	moderate Balmer absorption plus emission, spiral-like
e(a)	yes	≥ 4	...	strong Balmer absorption plus emission
e(b)	≥ 40	starburst
e(n)	AGN from broad lines or [OIII] 5007/H β ratio
e	yes	?	...	with at least one emission line but S/N too low to classify
?	?	?	...	unclassifiable
CSB	very blue	photometrically-defined starburst

TABLE 7
SPECTRAL SAMPLES

Cluster	N _{tot}	k	k+a	a+k	e(a)	e(c)	e(b)	e(n)	e	?
Full Sample										
Field	233	36	7	0	37	74	39	3	25	12
A 370	40	26	1	0	3	8	1	0	0	1
Cl 1447+26	21	7	1	0	6	6	1	0	0	0
Cl 0024+16	107	47	12	2	13	21	6	2	2	2
Cl 0939+47	71	31	13	6	7	10	2	1	1	0
Cl 0303+17	51	14	4	4	6	12	6	0	5	0
3C 295	25	10	6	1	2	2	0	3	1	0
Cl 0412–65	10	0	1	0	0	0	1	0	1	7
Cl 1601+42	58	33	15	0	4	3	2	1	0	0
Cl 0016+16	29	13	6	5	3	1	1	0	0	0
Cl 0054–27	12	5	1	0	0	1	0	0	3	2
Total	424	186	60	18	44	64	20	7	13	12
Morphological Sample										
Field	71	11	5	0	7	25	11	0	9	3
A 370	14	9	0	0	2	1	1	0	0	1
Cl 1447+26	10	4	0	0	2	3	1	0	0	0
Cl 0024+16	42	25	6	0	4	3	3	0	1	0
Cl 0939+47	31	16	6	2	5	2	0	0	0	0
Cl 0303+17	28	9	2	3	4	5	4	0	1	0
3C 295	20	7	5	0	2	2	0	3	1	0
Cl 0412–65	2	0	0	0	0	0	0	0	0	2
Cl 1601+42	28	20	5	0	0	1	1	1	0	0
Cl 0016+16	22	10	4	5	2	1	0	0	0	0
Cl 0054–27	7	4	0	0	0	0	0	0	1	2
Total	204	104	28	10	21	18	10	4	4	5

estimated in §4.1, which means that these differences could be larger, and, for example, the apparent peak in the luminosity distribution of e(a)'s in Fig. 7a may be partly an artifact of incomplete sampling. The difference between the k class and the fainter e(b) class is clearly significant: the likelihood that the two samples are drawn from the same luminosity distribution is only $\log_{10} P \sim -4.6$. Again, the difference may be larger still, owing to the incomplete sampling below ($M_V = -19 + 5 \log_{10} h$). We know of no selection effect in our study that would cause us to miss bright e(b) cluster galaxies. As we discuss in P98, the fact that the galaxies that we have identified as bursting are fainter than the other classes is significant, and discouraging for models that attempt to interpret these starbursts as progenitors for galaxies with strong Balmer lines in their spectra.

The cluster sample defined by our redshift measurements also allow us to unambiguously derive, for the first time, the absolute magnitude distributions as a function of morphology, again for $M_V \leq -19 + 5 \log_{10} h$. Fig. 7b shows a broad similarity between the absolute magnitudes of early- and mid-type disk systems (S0–Sa–Sb–Sc). Compared to these, elliptical galaxies show a systematically brighter distribution, and irregular galaxies exhibit a tail of fainter systems. These trends are in good agreement with what is seen in low-redshift clusters.

4.3. Morphological Properties of the Cluster Galaxies

What do the galaxies in our spectral classes look like? We illustrate the morphologies of the cluster members within each spectral class in Figs. 8. The general trend towards later-types in the active spectral classes is clear. The passive spectral classes are dominated by early-type galaxies, particularly ellipticals. The correspondence of morphology and spectral properties, the same as found for low-redshift analogs, indicates that a substantial fraction of the luminous ellipticals of these clusters was in place by $z \sim 0.5$ (Ellis et al. 1997, Dressler et al. 1997). The e(c) spectra are generally associated with disk galaxies, most of them familiar spirals and irregulars. This is true of some of the e(a)'s as well, but this class also includes many disk systems that look more disturbed than typical present-day spirals. The k+a/a+k class does include some elliptical galaxies, but the majority are disk galaxies, a few of which have an irregular or disturbed appearance. The significance of the correlation of morphology and spectral class are discussed further in B98.

¹³This tendency of intermediate-redshift disk galaxies to appear more asymmetric than low-redshift galaxies of similar type has been reported in essentially all studies of this type

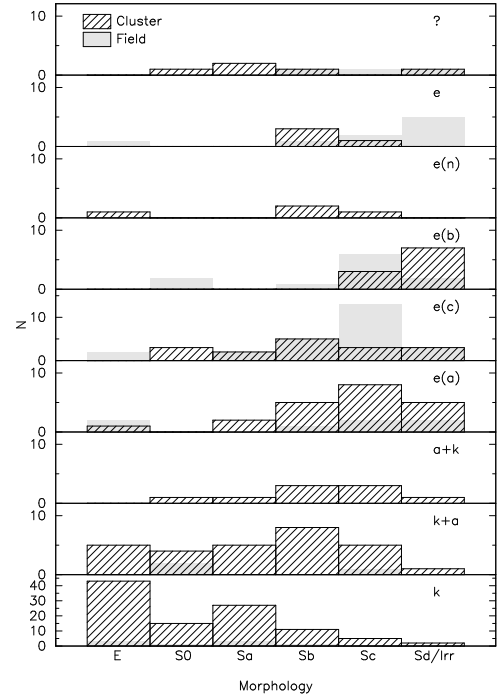


Fig. 10. A comparison of the distribution of morphological type within each spectroscopic class, for both cluster and field galaxies.

We briefly discuss evidence for interactions and mergers on the spectral classes of galaxies in our cluster samples. (We also comment on this issue in §5.2 which deals with the kinematics of the different cluster populations.) We show in Fig. 9a the distribution of disturbance class within the different spectral classes. The image disturbance, D , is a visual classification of the degree to which the galaxy's structure appears distorted or disturbed (S97) compared to a typical low-redshift galaxy of the same morphological type. The D class correlates well with the asymmetry of the galaxy's light profile (S97). Fig. 9a suggests that the spectral properties of the galaxies broadly correlate with the degree of image distortion and disturbance, the active and recently active populations having more galaxies classed as strongly asymmetric or distorted. However, looking at Fig. 9b we see an arguably stronger correlation between morphology and D with a pronounced shift towards higher D values in going to later-types (Sb–Sd/Irr). This could be due to a failure on our part to actually separate disturbance from a natural trend toward more irregular morphology for late-type systems, but the large number of $D \geq 2$ Sc galaxies (a type that is generally symmetric for low-redshift galaxies) suggests that the effect is real.¹³ If so, it most likely reflects the greater fragility of disks (compared to bulges) to perturbations, and the greater frequency of perturbations at higher redshift. However, we see that this effect does not appear to be result of the high density cluster environment: Fig. 9b shows that $50 \pm 8\%$ of the cluster Sb–Sc–Sd/Irr galaxies have $D \geq 2$, a proportion similar to that seen in the late-type field population, $60 \pm 11\%$. The same effect is seen at low-redshift (Hashimoto & Oemler 1999).

4.4. Spectroscopic Properties of the Cluster Galaxies

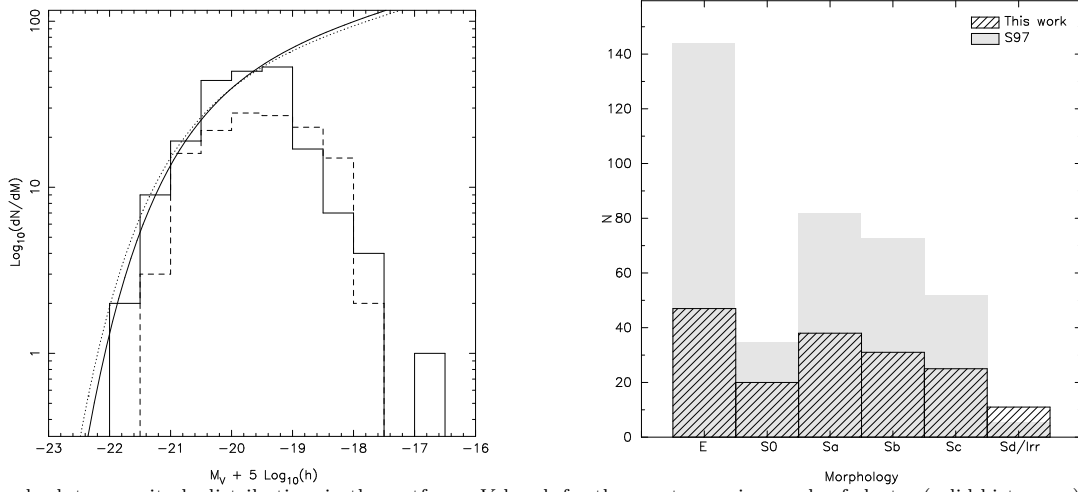


Fig. 6. a) The absolute magnitude distribution, in the restframe V -band, for the spectroscopic sample of cluster (solid histogram) and field (dashed histogram) galaxies (for those galaxies with DG92 photometry). The solid curve is the best-fit Schechter function to the cluster members, using a fixed faint-end slope of $\alpha = -1.25$. The characteristic luminosity derived from the fit is $M_V^* = -20.64 \pm 0.16 + 5 \log_{10} h$. The dotted line shows the fit to the luminosity functions derived from the morphological counts in the frames, corrected for field contamination (S97). This fit is shown for $\alpha = -1.25$ and with arbitrary vertical scaling. The good agreement of the two distributions shows that the spectroscopic catalog provides a representative luminosity distribution in the clusters at $M_V < -19 + 5 \log_{10} h$. b) The numbers of the different morphological types in the spectroscopic catalog (hatched histogram) brighter than $M_V = -19 + 5 \log_{10} h$. The filled histogram indicates the total numbers expected from the observed morphological counts in the clusters to the same depth, after correcting for field contamination (see S97).

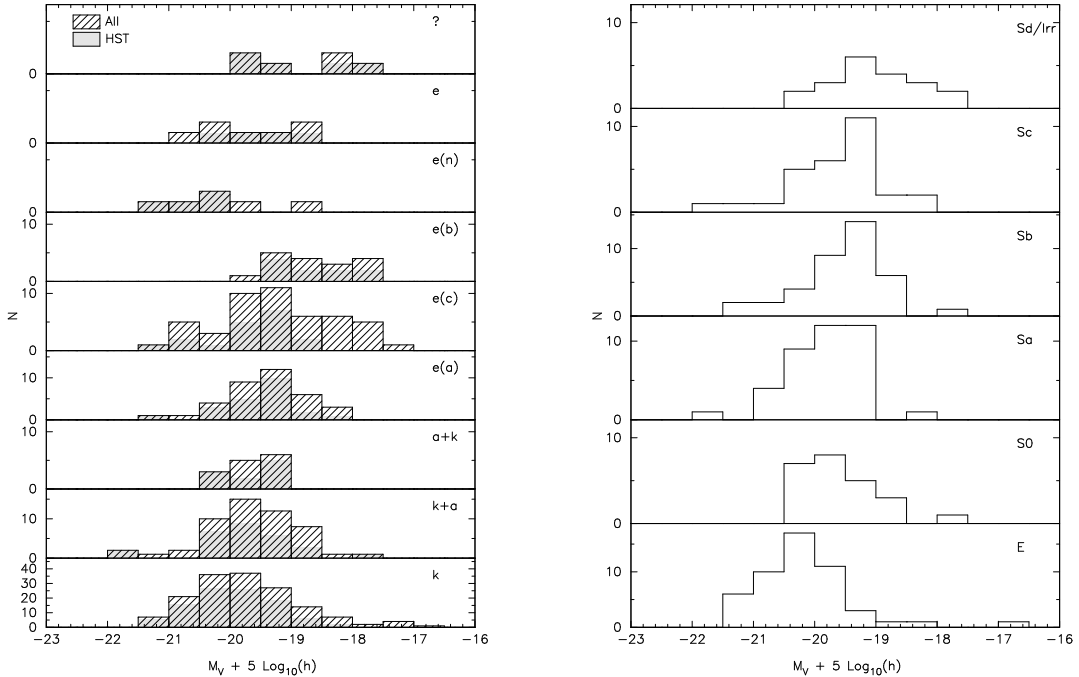


Fig. 7. a) The absolute magnitude distribution in the restframe V -band for cluster members separated into the different spectroscopic classes for both the HST fields and the full sample. In this panel we convert the ground-based r -band photometry to rest-frame V -band. b) The same distribution, but now separated on morphological type and using the HST photometry. The K -correction applied in both cases assumes a spectral energy distribution (SED) similar to a local Sbc galaxy, this introduce a typical systematic error of only ~ 0.06 mags for E/S0 and Sd/Irr SEDs.

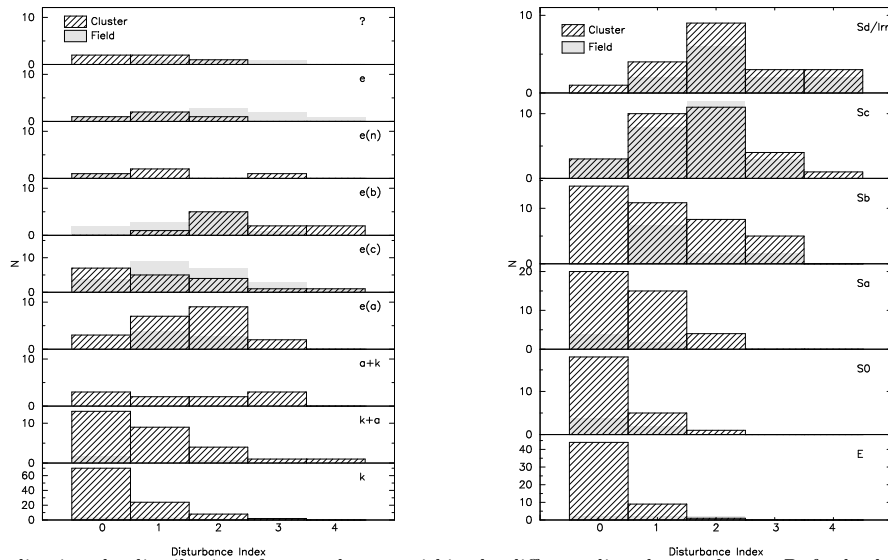


Fig. 9. a) Histograms indicating the distribution of spectral types within the different disturbance classes, D , for both cluster and field populations (hatched and filled histograms respectively). $D \geq 2$ denotes strongly asymmetric or disturbed light distribution. b) The numbers of galaxies in the different disturbance classes as a function of galaxy morphology. Note the broad similarity of the cluster and field distributions for the later-type spiral galaxies.

In Fig. 10 we quantify the distribution of morphological type for the various spectral classes, for both cluster members *and* field galaxies. The strong, though broad, relation between morphology and star-formation seen in low-redshift galaxies is present in this intermediate redshift sample as well. Looking at the star-forming population which causes the Butcher-Oemler effect we see a clear tendency for these galaxies to be predominantly late-type systems (Couch et al. 1994, 1998; Dressler et al. 1994; Oemler et al. 1997), although here there is a tail of earlier-types (at least in the e(a) and e(c) classes). These active early-type (E and S0) galaxies comprise a higher fraction of the field population than they do in the clusters. The two “recently-active” classes, k+a and a+k, appear to have morphological distributions which are intermediate between the passive and active cluster populations. There seems to be a clear distinction between k+a and a+k in the sense that the latter are of later morphological type, though the small number of a+k types limits the statistical certainty of this result.

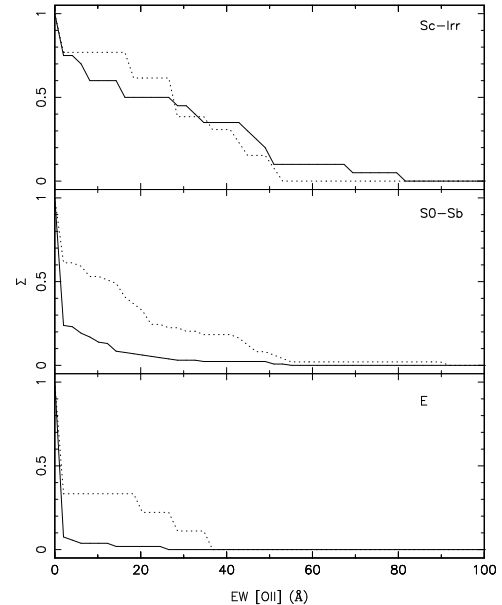


Fig. 11. The cumulative distribution of [OII] 3727 EW for three independent morphological bins for both cluster (solid line) and field (dotted line) populations.

It is interesting that, although the passive cluster population is dominated by elliptical and S0 galaxies, there is a significant number of later types, stretching out to Sd/Irr, which also show no emission lines. Aperture biases in our spectroscopy are unlikely to explain the lack of observed star-formation in this group: the spectra sample the central $\sim 65h^{-2}$ kpc² of these distant galaxies. Further support for a lack of on-going star-formation in these systems is shown by the uniform red colors of those galaxies for which we have imaging in two passbands with *WFPC2*.

We quantify the occurrence of passive late-type galaxies, and compare cluster and field populations, in Fig. 11. Using the cumulative distribution of [OII] 3727 EW, we find that for the morphological groups E and S0–Sb there is a significantly higher fraction of galaxies showing little or no [OII] emission in clusters as compared to the field. The likelihood, P , that the cluster and field samples are drawn

from the same population is less than $\log_{10} P < -2.4$ for both E and S0–Sb samples. However, the comparison of the [OII] distribution of the latest-type systems (Sc–Irr, T=7–10) shows no significant difference between the cluster and field, although the number of galaxies is somewhat smaller.

As an overall trend, then, there seems to be a decline in current star-formation at a fixed Hubble-type from field to cluster (see also Balogh et al. 1998). Furthermore, based on [OII] EW alone as a measure of star formation, we see no evidence for enhanced star-formation in gas-rich cluster galaxies compared to the equivalent morphological sample in the field. We discuss this incidence of passive late-type galaxies further in P98.

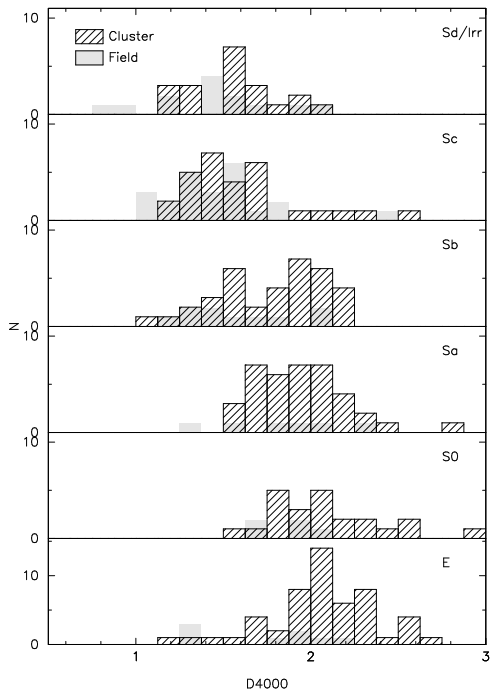


Fig. 12. A comparison of the distribution of D4000 measures in the different morphological types, for both cluster and field galaxies.

In contrast to these results based on [OII] EW, the distribution of D4000 strengths (Fig. 12) is very similar for cluster and field: the individual morphological types are indistinguishable in D4000 at better than $\log_{10} P > -1$ in each case. Thus, while [OII], the tracer of current star-formation, shows a decline in the cluster, this does not appear to be reflected in an index sensitive to the star-formation averaged over a somewhat longer period of the recent past (~ 1 –3 Gyrs).

5. RESULTS AND DISCUSSION

5.1. The Incidence of $k+a/a+k$ and $e(a)$ Galaxies

Our spectral catalog exhibits one effect that is especially strong: the incidence of $k+a/a+k$ galaxies in distant clusters is very high compared to the surrounding field. Table 7 shows that in the cluster sample we have 60 examples of $k+a$ and 18 examples of $a+k$, totaling 18% of the sample. This is similar to the typical value of ~ 10 –20% found by magnitude-limited surveys of distant clusters (DG92;

Couch et al. 1998). However, this value strongly contrasts with the 7 occurrences, all $k+a$, found in the high-redshift field sample, only 2%.

Indeed, 4 of these 7 cases are either uncertain or borderline, a far greater fraction than for the cluster sample, so an incidence of $\sim 1\%$ is compatible with these data. For the low-redshift Las Campanas Redshift Survey (hereafter LCRS), Zabludoff et al. (1996) found an incidence of 0.2%, but their selection criteria included a stronger limit on $H\delta$ of 5.5 Å and they note that the number increases to 0.6% when the limit is dropped to 4.5 Å. Hashimoto (1998) has evaluated the occurrence of the spectral classes as defined in this paper for the LCRS, and finds 2.3% for the occurrence of $k+a/a+k$ types. In summary, these data seem to point to at most a factor two increase in the frequency of $k+a/a+k$ types between the low- and intermediate-redshift field populations. This is in marked contrast to the order-of-magnitude increase in the frequency of $k+a$ types in rich clusters. At low redshift, this frequency is $\lesssim 1\%$ (determined using the Dressler and Shectman (1988) catalog), compared to the 18% found here for the $z \sim 0.5$ clusters.¹⁴

Zabludoff et al. attributed many of the low-redshift field “E+A’s” as due to mergers and strong interactions, since morphologies of this type are often observed in the low-redshift examples. The expected evolution can be estimated from the change in the incidence of close pairs (Zepf & Koo 1989; Patton et al. 1997), which would be predicted to be the parent population. Patton et al. (1997) claim that the proportion of close pairs (two galaxies within $20h^{-1}$ kpc) increases by a factor of ~ 1.5 between $z = 0$ and $z = 0.33$. Extrapolating this behavior to $\langle z \rangle = 0.42$ would predict an increase in the fraction of close pairs of ~ 2 –3 over that seen locally. Although we see at most a factor of two increase in the $k+a$ population from low to high redshift using the LCRS and our sample, this does not rule out that a significant fraction of field $k+a$ ’s are due to such mergers.

Zabludoff et al. argue further that, as the merger/interaction mechanism appears to be responsible for low-redshift field examples of such galaxies, it is reasonable to conclude that mergers may also be responsible for the $k+a/a+k$ galaxies in the intermediate-redshift clusters. However, the radically different evolution described above of the $k+a/a+k$ population between cluster and field environments suggests that the cluster environment is crucial in either the formation of *cluster* $k+a/a+k$ galaxies, or in prolonging their visibility. This could in part be due to an increased propensity for mergers in the groups infalling into the intermediate-redshift clusters. However, our morphological analysis (S97) finds only a minority of cases of $k+a$ spectra where the galaxy shows signs of a classic two-body merger, as Zabludoff et al. found for the low-redshift field examples. We conclude, then, that at least one mechanism other than mergers is responsible for the large fraction of $k+a/a+k$ galaxies in intermediate-redshift clusters.

As we discuss in B98, the majority of $k+a/a+k$ spectra are the result of a sudden decline in star formation

¹⁴Caldwell & Rose (1997) have reported a frequency of $\sim 15\%$ of notably stronger Balmer lines in early type galaxies in five low-redshift clusters. These are for the most part lower luminosity systems, with $H\delta < 3.0$ Å, which the authors suggest are the remnants of earlier bursts. The results of that study do not, therefore, conflict with the much lower frequency found by Dressler and Shectman for stronger, more luminous systems.

rate that followed a substantial rise, or burst, of star-formation, leaving a population of A-stars to dominate the light for $\sim 10^9$ years. Given the generic nature of the star-formation history required to form an a+k/k+a, mergers are obviously not a unique explanation for the k+a/a+k phenomena. For example, accretion of smaller satellites, instead of mergers of comparable mass systems, is not inconsistent with the morphologies we see. The greater fraction of a+k/a+k galaxies in the intermediate-redshift clusters as compared to the field is likely to be connected as well with the frequency of e(a) galaxies in these environments (B98).

5.2. The Distribution and Kinematic Properties of the Cluster Galaxies

As a final exercise in the comparison of spectroscopic properties with other cluster characteristics, we examine the radial distributions of our cluster sample as a function of spectroscopic type. We begin by assigning field centers — these positions are given in Table 2. There is usually little ambiguity of this due to the presence of a D or cD galaxy, these have been confirmed as the cluster centers in all cases from our the weak lensing analysis in Smail et al. (1997b). Even in more complex cases, such as Cl 1447+26, the ambiguity in choosing a center will play little role over the large range in radius we investigate.

Fig. 13. The cumulative radial distribution of different spectral types. These are shown for the all members from the whole sample which have $M_V < -19 + 5 \log_{10} h$. There is a clear difference between the radial distribution of k, k+a/a+k, and e type galaxies, with the former being most concentrated, the latter the least. The k+a/a+k class seems to be intermediate between the two showing a similar decline to the k types on the outskirts of the cluster, but a flatter distribution in the core, more in keeping with that seen for the e types.

In Fig. 13 we show for the combined clusters the cumulative radial distribution for different spectroscopic types. This procedure is crude because it averages over the non-spherical distribution of galaxies within the clusters, but it may provide some insight into the characteristic distributions of different classes of galaxies. Not surprisingly, the k types, generally made up of E and S0 galaxies (Fig. 10), but including significant early-type spirals as well, are the most concentrated population in these clusters (c.f. S97). Also, not surprisingly, the emission line galaxies strongly avoid the center ($r \leq 50h^{-1}$ kpc) of these clusters and have

a much more extended distribution. What is perhaps more interesting is the way the k+a/a+k types, which may sensibly interpreted as post-starburst galaxies, avoid the centers in contrast to the k types, but are far less extended than the emission-line galaxies.¹⁵ The near absence of k+a types in the field, discussed above, coupled with the sudden rise in their frequency as the cluster center is approached, with an almost complete demise in the central regions, appears to be clear evidence for the environment effecting either their formation or visibility.

We note in passing that a similar diagram subdividing the e types into e(a), e(c), and e(b) shows no significant difference, though there is a hint that the e(a) class has a slightly more extended distribution.

We now investigate the rudimentary kinematics of the sample of cluster members. In Table 8 we list the restframe velocity dispersions and uncertainties for the entire cluster sample broken down in terms of morphological type, spectral class, disturbance and activity class (the latter three sections refer only to those galaxies lying within the *WFPC2* fields). The distributions for the spectral and morphological types are also shown in Fig. 14. These values are calculated using the mean cluster redshifts listed in Table 2 and are simple averages across the cluster (no allowance has been made for different velocity dispersion for the different clusters — when such corrections are applied they make no qualitative change to the conclusions listed below). The uncertainties in the velocity dispersions are 1σ values estimated from bootstrap resampling of the observed distributions.

Starting with the morphological samples in Table 8 we see a marked difference between the velocity dispersion of the elliptical galaxies and all the later-types, the latter having higher dispersions (including the S0 galaxies). A similar difference is noticeable when the sample is split into different spectral classes (now including the whole spectroscopic catalog of members). Interestingly the galaxies whose spectra were too poor to be classified, the “?” class, show the lowest dispersion — suggesting that these may be predominantly passive, cluster galaxies.

The strongest trend is the significantly higher velocity dispersion of the presently or recently star-forming systems compared to the passive population (c.f. Dressler 1986). In particular, combining the different spectral classes (e(all) comprises e(a)/e(b)/e(c)/e(n)/e) from Table 8 we find that the emission-line and k-type galaxies have relative dispersions of $\sigma_{em}/\sigma_k = 1.40 \pm 0.16$, with the k+a/a+k galaxies being intermediate between the two. The higher dispersions of the active populations are consistent with these galaxies being less virialised than the k-type population. Such a trend can also be discerned in the variation of velocity with activity (as traced by the [OII] EW) *within* the individual morphological types. Splitting each of the more active morphological classes (Sb-Sd/Irr) at its median [OII] EW into “low” and “high” activity samples we find the dispersions listed at the bottom of Table 8 for the different morphological samples. For all three morphological types, the more active sample shows the higher velocity dispersion. A higher velocity dispersion is often taken as a sign of an infalling population, but, as we discuss below,

¹⁵It is tempting to describe this distribution as a “thick shell”, but we consider this potentially misleading due to the substantial departures from spherical symmetry exhibited by our clusters. Rather, it is probably more instructive to think of k+a/a+k types occurring most frequently at an intermediate radius $R \sim 200kpc$.

TABLE 8
VELOCITY DISPERSIONS OF CLUSTER POPULATIONS

Sample	N	$\langle v \rangle$ (km s^{-1})	σ (km s^{-1})	$\delta\sigma$ (km s^{-1})
Morphological Types				
E	50	-109.9	974.9	78.7
S0	24	-378.7	1709.7	374.1
Sa	39	34.3	1336.5	137.2
Sb	38	179.5	1290.6	147.7
Sc	29	640.9	1212.6	219.2
Sd/Irr	20	-323.2	1894.6	231.9
Spectral Classes				
k	186	12.5	1064.8	55.2
k+a	60	105.4	1421.6	204.9
a+k	18	120.9	1236.4	223.7
e(a)	44	-27.2	1420.9	151.3
e(c)	64	-226.4	1437.1	126.2
e(b)	20	-168.8	1740.1	260.9
e(n)	7	576.1	1495.3	404.9
e	13	743.2	1400.1	288.8
?	12	367.6	694.1	116.3
k	186	12.5	1064.8	55.2
k+a/a+k	78	109.0	1373.4	172.4
e(all)	148	-36.3	1486.0	90.1
Disturbance Classes				
$D = 0$	100	-33.9	1252.9	144.9
$D = 1$	54	207.6	1382.8	146.2
$D = 2$	34	58.9	1417.5	202.3
$D = 3$	12	307.5	1572.1	329.4
$D = 4$	4	-681.9	2884.3	807.8
Activity Classes				
Sb-high	10	...	1429.5	294.1
Sb-low	28	...	1265.5	173.6
Sc-high	14	...	1293.7	334.2
Sc-low	15	...	1084.2	246.1
Sd-high	10	...	2274.5	332.7
Sd-low	10	...	1243.1	238.1

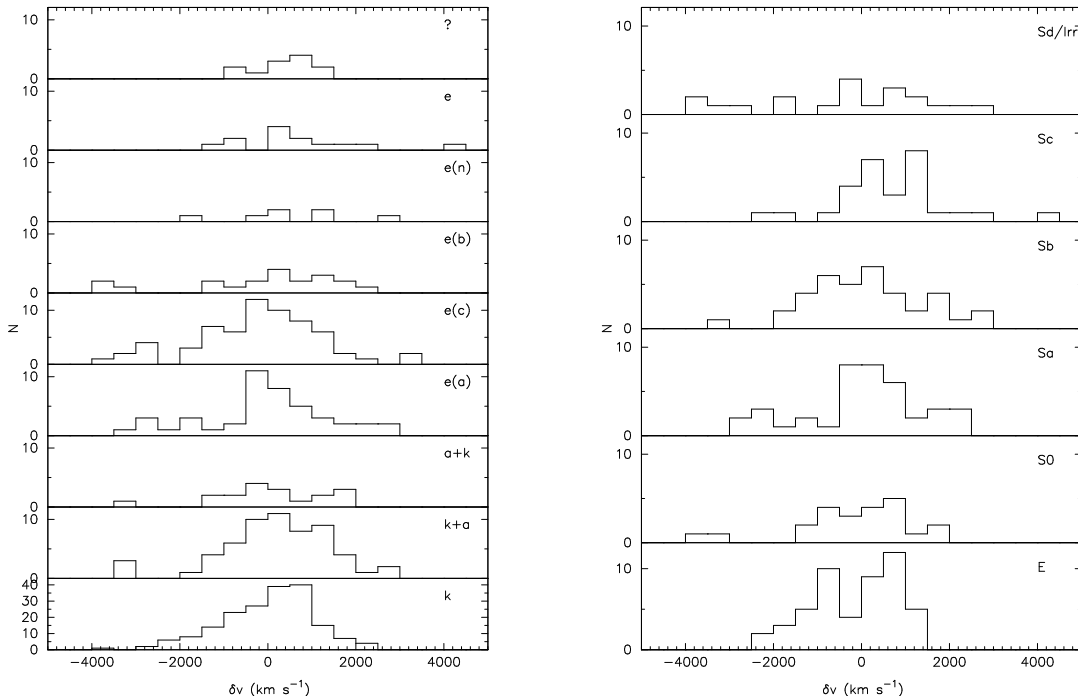


Fig. 14. a) The restframe velocities of cluster members, calculated relative to their respective cluster means (Table 2). These histograms are shown for the different spectroscopic classes. No scaling has been applied when combining the distributions from different clusters. b) The restframe velocities of cluster members, relative to their respective cluster means. These histograms are shown for the different morphological types.

including spatial information in our analysis shows only weak evidence for infall.

We note that the [OII] EW distributions for these active cluster members do not show any enhanced activity over that seen in the surrounding field for any given morphological type (c.f. §4.2). Apparently, then, the observed correlation of velocity dispersion and activity (as measured by [OII] EW) is not triggered by a mechanism which causes the higher star-formation rates due to the high relative velocities of the galaxies within the clusters (i.e. ram-pressure induced star-formation). We suggest instead that the correlation between activity and velocity dispersion reflects a decline in star-formation in the galaxies which runs in parallel with and is causally linked their virialization within the clusters. In this regard we also mention the trend for more disturbed galaxies to have higher velocity dispersions, Table 8, a result which remains when we restrict the analysis to late-type galaxies, Sb–Irr.

We next combine the velocity and positional information for the entire sample of clusters, focusing on the spectral classes, to calculate the velocity dispersion as a function of spectral class and radius. Dressler (1986) used the Giovanelli and Haynes (19ZZ) catalog of spirals in nearby clusters to show that gas-poor spirals tend to travel on radial orbits that take them into the cluster center, as compared to the more isotropic orbits of the gas-rich spirals. Here we divide the k, k+a/a+k, and emission-line classes into three bins of radial position, each containing one-third of their respective samples. The resulting velocity dispersions are shown in Fig. 15.

Fig. 15. The velocity dispersions of the different spectral types, averaged over the entire sample, as a function of radius. The velocity dispersion is everywhere higher for active systems compared to passive galaxies. Note that the k+a/a+k types exhibit a peak in velocity dispersion that may be related to their distinctive spatial distribution.

Unlike the clear difference in the orbital properties of gas-deficient systems in nearby clusters, our sample exhibits ambiguous evidence at best. The k and e types both have velocity dispersion that falls gently with radius or are, within the errors, flat. This suggests populations on mildly radial orbits, possibly an infalling population, or a simple isothermal distribution. More puzzling is the peak in velocity dispersion for the k+a/a+k types, which does appear to be statistically significant. It is possible, of course, that higher velocities increase the chance of producing a k+a/a+k. It is also possible that this kinematic feature is connected with their unusual radial distribution,

as mentioned above. A system of largely circular orbits that might characterize this distribution, which is concentrated like the k-types but avoids the core, would appear to have a higher velocity dispersion due to projection of what are largely tangential velocities. This is, however, not consistent with the idea that such galaxies derive from an infalling population on what are basically radial orbits. At this point, the statistics are poor enough, and the range of models so broad, that it is not worthwhile to explore this further here.

6. CONCLUSIONS

- We have presented detailed spectroscopic observations of 657 galaxies in the fields of 10 $z = 0.37$ – 0.56 clusters. Combining these with our detailed *HST*-based morphological catalogs in these fields we construct samples of 204 cluster members and 71 field galaxies with both accurate spectral and morphological information.
- Using observational and theoretical justifications we have constructed a new quantitative spectral classification scheme and use this to interpret correlations between our spectral information and other properties of the galaxies in our catalog.
- Based upon an analysis of the [OII] EW distributions, we find no evidence for an increase in the occurrence of strongly star-forming galaxies in the moderate-redshift cluster environment compared to the moderate-redshift field using morphologically-selected samples. However, we do find a large population of late-type cluster, but not field, galaxies which show little or no evidence of on-going star-formation.
- This passive, late-type cluster population is related to our spectral classes k+a/a+k, both of which we interpret as indicative of post-starburst behavior. Galaxies with k+a/a+k spectra are an order-of-magnitude more frequent in the cluster environment compared to the high redshift field.
- These k+a/a+k galaxies avoid the central regions of the clusters, in contrast to the k types, but are also far less extended than the emission-line galaxies, and much less common in the field. This appears to be clear evidence for the environment effecting either their formation or visibility.
- A detailed analysis of the spectroscopic and morphological information discussed here will be presented in Poggianti et al. (1998).

ACKNOWLEDGEMENTS

We thank Ray Lucas at STScI for his enthusiastic help which enabled the efficient gathering of these HST observations. BMP and HB warmly thank Steve Maddox for crucial help during the 1995 WHT run and in the subsequent reduction of those data. We also thank Alfonso Aragón-Salamanca, Nobuo Arimoto and Amy Barger for useful discussions and assistance. AD and AO acknowledge support from NASA through STScI grant 3857. IRS acknowledges support from a PPARC Advanced Fellowship and from Royal Society and Australian Research Grants while an Honorary Visiting Fellow at UNSW. WJC acknowledges support from the Australian Department of Industry, Science and Technology, the Australian Research Council and Sun Microsystems. This work was supported in part by

the Formation and Evolution of Galaxies network set up by the European Commission under contract ERB FMRX-CT96-086 of its TMR program. We acknowledge the avail-

ability of the Kennicutt's (1992) atlas of galaxies from the NDSS-DCA Astronomical Data Center.

REFERENCES

- Allington-Smith, J. R., et al., 1994, *PASP*, 106, 983
 Abraham, R., et al., 1996, *ApJ*, 471, 694
 Aragón-Salamanca, A., Ellis, R. S., Couch, W. J., & Carter, D., 1993, *MNRAS*, 262, 764
 Balogh, M. L., Schade, D., Morris, S. L., Yee, H. K. C., Carlberg, R. G., & Ellingson, E., 1998, *ApJL*, 504, L75.
 Barger, A. J., Aragón-Salamanca, A., Ellis, R. S., Couch, W. J., Smail, I., & Sharples, R. M., 1996, *MNRAS*, 279, 1
 Barger, A. J., Aragón-Salamanca, A., Smail, I., Ellis, R. S., Couch, W. J., Dressler, A., Oemler, A. Jr, Butcher, H., & Sharples, R. M., 1998, *ApJ*, in press.
 Bothun, G. D., & Gregg, M. D., 1990, *ApJ*, 350, 73
 Butcher, H., & Oemler, A. Jr, 1978, *ApJ*, 279, 18
 Butcher, H., & Oemler, A. Jr, 1984, *ApJ*, 285, 426
 Caldwell, N., & Rose, J. A., 1997, *AJ*, 113, 492
 Couch, W. J., & Sharples, R. M., 1987, *MNRAS*, 229, 423 (CS87)
 Couch, W. J., Ellis, R. S., Sharples, R. M., & Smail, I., 1994, *ApJ*, 430, 121
 Couch, W. J., Barger, A. J., Smail, I., Ellis, R. S., Sharples, R. M., & Smail, I., 1998, *ApJ*, 497, 188
 Dressler, A., 1986, in *Nearly Normal Galaxies*, ed. S. M. Faber, pp. 276.
 Dressler, A., & Shectman, S. A., 1987, *AJ*, 94, 899.
 Dressler, A., & Shectman, S. A., 1988, *AJ*, 95, 284.
 Dressler, A., & Gunn, J. E., 1983, *ApJ*, 270, 7.
 Dressler, A., & Gunn, J. E., 1992, *ApJS*, 70, 1 (DG92)
 Dressler, A., Oemler, A. Jr., Butcher, H., & Gunn, J. E., 1994, *ApJ*, 430, 107
 Dressler, A., Oemler, A. Jr., Couch, W. J., Smail, I., Ellis, R. S., Barger, A., Butcher, H., Poggianti, B. M., & Sharples, R. M., 1997, *ApJ*, 490, 577.
 Ellis, R. S., Smail, I., Dressler, A., Couch, W. J., Oemler, A., Butcher, H., & Sharples, R. M., 1997, *ApJ*, 483, 582
 Franx, M., 1993, *ApJL*, 407, L5
 Fisher, D., Fabricant, D., Franx, M., van Dokkum, P., 1998, *ApJ*, in press
 Giovanelli, & Haynes, 1992, *ZZZ*
 Hashimoto, Y., Oemler, A. Jr, 1999, *ZZZ*
 Hashimoto, Y., 1998, private communication.
 Kennicutt, R. C. Jr, 1992, *ApJS*, 79, 255
 Kells, W., Dressler, A., Sivaramakrishna, A., Carr, D., Koch, E., Epps, H., et al., 1998, *PASP*, submitted.
 Lavery, R. J., & Henry, J. P., 1994, *ApJ*, 426, 524
 Lubin, L. M., 1996, *AJ*, 112, 23
 Oemler, A., Dressler, A., & Butcher, H. R., 1997, *ApJ*, 474, 561
 Patton, D. R., Pritchet, C. J., Yee, H. K. C., Ellingson, E., Carlberg, R. G., 1997, *ApJ*, 475, 29
 Poggianti, B. M. et al., 1998, in preparation (P98)
 Rakos, K. D., & Schombert, J. M., 1995, *ApJ* 439, 47
 Rakos, K. D., Odell, A. P., & Schombert, J. M., 1997, *ApJ*, 490, 194
 Smail, I., Ellis, R. S., Dressler, A., Couch, W. J., Oemler, A. Jr, Butcher, H., & Sharples, R. M., 1997a, *ApJ*, 479, 70
 Smail, I., Dressler, A., Couch, W. J., Ellis, R. S., Oemler, A. Jr, Butcher, H., & Sharples, R. M., 1997b, *ApJS*, 110, 213 (S97)
 Smail, I., Edge, A. C., Ellis, R. S., & Blandford, R. D., 1998, *MNRAS*, 293, 124
 Stanford, S. A., Eisenhardt, P. R., & Dickinson, M. E., 1995, *ApJ*, 450, 512
 Stanford, S. A., Eisenhardt, P. R., & Dickinson, M. E., 1998, *ApJ*, in press.
 Zabludoff, A. I., Zaritsky, D., Lin, H., Tucker, D., Hashimoto, Y., Shectman, S. A., Oemler, A. Jr., Kirsher, R. P., 1996, *ApJ*, 466, 104.
 Zepf, S. E., Koo, D. C., 1989, *ApJ*, 337, 34
 Zijlstra, A., Giraud, E., Melnick, J., Dekker, H., & D'Odorico, S., 1996, ESO Operating Manual, version 3.0, ESO.

Fig. 8a. The images of those galaxies in our sample lying within the *WFPC2* frame, grouped into spectroscopic classes. This first panel shows those galaxies with k spectral types. Each image is $5'' \times 5''$ (or $15.5\text{--}18.6 h^{-1}$ kpc depending upon the cluster's redshift) and has the same orientation as the *HST* field (S97). The cluster and galaxy ID from the *WFPC2* catalogs (from Tables 4 in S97, or Table 4a below) and the spectral class and morphological type are marked on each frame. For the plates in Fig. 8 see <http://www.ociw.edu/~irs/morphs2.html#figs>

Fig. 8a. continued.

Fig. 8a. continued.

Fig. 8b. The k+a sample.

Fig. 8c. The a+k sample.

Fig. 8d. The e(a) sample.

Fig. 8e. The e(c) sample.

Fig. 8f. The e(b) sample.

Fig. 8g. The e(n) sample.

